Status of the Dielectric Constant of Sea Water at L-Band for Remote Sensing of Salinity

David M. Le Vine, *Life Fellow, IEEE*, Roger H. Lang, *Life Fellow, IEEE*, Yiwen Zhou, *Member, IEEE*, Emmanuel P. Dinnat, *Senior Member, IEEE*, and Thomas Meissner, *Senior Member, IEEE*

***Abstract*— The model expressing the dielectric constant of sea water at microwave frequencies as a function of salinity and temperature is an important element in remote sensing of sea surface salinity. It is also important independently as a description of the physical properties of salt water. A major milestone was the development in the late 1970s by Klein and Swift of a model based on laboratory measurements at L- and S-band and a functional form supported by theory for polar molecules and previous work on freshwater. Much of the subsequent work has focused on measurements at higher frequency and determining model parameters tuned to apply for applications, such as remote sensing of sea surface temperature (SST). Interest in the dielectric constant at 1.4 GHz (L-band) increased again with the development of soil moisture ocean salinity (SMOS) and Aquarius to measure salinity from space, but there have been few new measurements at L-band and often confusion regarding the applicability of new models at 1.4 GHz. The objective of this article is to compare available models in the context of how well they represent the dielectric constant of sea water at 1.4 GHz. Among the criteria applied will be the recent measurements at the George Washington University of the dielectric constant at 1.4 GHz.**

***Index Terms*— Dielectric constant, L-band, microwave remote sensing, ocean salinity, sea water.**

I. Introduction

A MODEL for the dielectric constant of water as a function of salinity and temperature is an essential element in remote sensing of parameters of the ocean surface, such as salinity and temperature. The beginning of passive microwave remote sensing of the oceans in the 1970s [1], [2] increased the importance of a good model. A major milestone was the development of a model for saltwater by Klein and Swift [3] based on laboratory measurements at L- and S-band and employing a functional dependence on frequency based on the response of polar molecules [4], [5]. Most of the work on the dielectric constant of sea water afterward was done to extend the model to higher frequencies [6], [7], [8], [9], [10], [11] for applications, such as remote sensing of sea surface temperature (SST), but the development of sensors to measure sea surface salinity (SSS) from space, such as soil moisture ocean salinity (SMOS) [12], [13] and Aquarius [14], motivated new work at L-band, including new measurements [15], [16] and new models [15], [17], [18], [19].

Research on the microwave response of the water molecule [4] established the functional form for the dielectric constant, and as a result, all the models are similar in their functional dependence on frequency. Mathematically, they can all be evaluated at any frequency and they are remarkably similar from 1 to 100 GHz. The result is a plethora of models with similar features but fitted to measurements covering a varying range of frequency, temperature, and salinity. To apply the models without regard to the limitation set by the data used in fitting the model can lead to misrepresentation and error in the retrieval of science products. This is especially the case in remote sensing of salinity, where high accuracy is required on both the radiometer (e.g., 0.1 K) and the model for the dielectric constant (0.25%) [20].

The objective of this article is to take a close look at the models for the dielectric constant of sea water in the context of remote sensing of SSS and how well they represent the dielectric constant of sea water at 1.4 GHz. These are not necessarily identical criteria as some models are tuned to optimize remote sensing, such as [10], [11], and [19], and others are tuned to fit laboratory measurements of the dielectric constant [3], [7], [17]. The success of a model in remote sensing is not necessarily a measure of its accuracy representing the dielectric constant of sea water. This is so because empirical adjustments in the retrieval algorithm can hide errors in the model for emission from the surface. In the following sections, nine models reported in the literature for the dielectric constant of sea water will be compared at 1.4 GHz. It will be clear that some of the models should not be used at L-band. The remainder will be compared with the laboratory measurements at GWU [15], [17] to assess their representation as a function of temperature and salinity of the dielectric constant of sea water. In Section II, a brief introduction will be given to the

Manuscript received 29 April 2022; revised 16 August 2022; accepted 12 September 2022. Date of publication 19 September 2022; date of current version 7 October 2022. The work of Yiwen Zhou and Roger H. Lang was supported by the National Aeronautics and Space Administration (NASA) through the Physical Oceanography Program under Grant NN17AK01G and Grant NNG05GO48G. The work of Emmanuel P. Dinnat was supported by NASA under Grant 80NSSC22K0215. *(Corresponding author: David M. Le Vine.)*

David M. Le Vine is with the Cryospheric Sciences Laboratory, NASA Goddard Space Flight Center, Greenbelt, MD 20771 USA (e-mail: david.m.levine@nasa.gov).

Roger H. Lang is with the Electrical and Computer Engineering Department, The George Washington University, Washington, DC 20052 USA (e-mail: lang@gwu.edu).

Yiwen Zhou is with the Swiss Federal Institute for Forest, Snow and Landscape Research WSL, CH-8903 Birmensdorf, Switzerland (e-mail: yiwen.zhou920@gmail.com).

Emmanuel P. Dinnat is with the Cryospheric Sciences Laboratory, NASA Goddard Space Flight Center, Greenbelt, MD 20771 USA, and also with the Center of Excellence in Earth Systems Modeling and Observations, Chapman University, Orange, CA 92866 USA (e-mail: emmanuel.dinnat@nasa.gov).

Thomas Meissner is with Remote Sensing Systems, Santa Rosa, CA 94501 USA (e-mail: meissner@remss.com).

Digital Object Identifier 10.1109/TGRS.2022.3207944

functional form of the models of the dielectric constant of sea water. The models are described in Sections III and IV and they are compared as a function of frequency and compared at 1.4 GHz as a function of salinity and temperature. A comparison by model component (e.g., conductivity, relaxation time, and static limit) is given in Appendix I. In Section V, the models are compared against the laboratory measurements at 1.4 GHz. The implications with respect to remote sensing and the representation of the dielectric constant of sea water are discussed in Section VI.

II. Background: The Model Function

The dielectric constant of sea water consists of two parts, a contribution due to orientation and/or distortion of the water molecule (called "polarization" [5], [21]) and a contribution due to motion of charge (current). Theory for the polarization of an ideal polar molecule in a viscous (i.e., damping) medium was developed by Debye [4] and Somaraju and Trumpf [5], and experimental evidence supports this solution for water [22], [23]. All the models discussed here employ this form for the frequency dependence. About half the models examined here employ one Debye "resonance" and half employ a second resonance as suggested by Stogryn *et al.* [6] to get a better fit at higher frequency. Adding salt to water makes the liquid conducting, necessitating an additional term to account for the current. The model with two resonances has the following form:

$$\varepsilon = \varepsilon_\infty + \frac{\varepsilon_s - \varepsilon_1}{1 + j\omega\tau_1} + \frac{\varepsilon_1 - \varepsilon_\infty}{1 + j\omega\tau_2} - j\frac{\sigma}{\omega\varepsilon_o} \tag{1}$$

where f is the frequency, ε_o is the permittivity of vacuum, and the other parameters, such as conductivity, σ, relaxation times, τ_1 and τ_2, and static limit, ε_s, are to be determined from measurements. In those models with a single resonance, ε_1 is replaced by ε_∞.

Measurements suggest a relaxation time for the first resonance near $\tau_1 = 0.05$ ns (near 20 GHz) depending on temperature [22], [24]. Models employing a second resonance have resonant frequencies above 100 GHz and for applications at the low end of the microwave spectrum, for example at 1.4 GHz for remote sensing of SSS, the first resonance is dominant. Most models intended for use specifically near 1.4 GHz only include the first Debye resonance term.

Since the model for the dielectric constant should reduce to fresh water when $S = 0$, it can be argued that the static term, ε_s, can be written in the following form:

$$\varepsilon_s = A(T)\{1 - B(T)S\} \tag{2}$$

where $A(T)$ and $B(T)$ are the functions to be determined. This form was used by Guillou *et al.* [9] and adopted by Boutin *et al.* [19] as suggested by Somaraju and Trumpf [5]. The form was also adopted in the recent model of Zhou *et al.* [17] but with B dependent on salinity [i.e., $B = B(S, T)$]. Zhou *et al.* [17] found that using this constraint reduced the number of unknowns and resulted in a better fit than an earlier model, which attempted a third-order polynomial in S and T for the static term [15].

The last term in (1) follows from the definition of current: that is, a macroscopic model with the assumption that the motion of charge is proportional to the electric field with a proportionality constant called conductivity, σ. The definition of "practical salinity" in terms of conductivity established a relationship between salinity, temperature, and conductivity [25]. Stogryn *et al.* [6] inverted this definition to establish the model, $\sigma(S, T)$, needed in (1). This inversion has been revisited and is available as public code [47]. The models by Meissner and Wentz [10], [11] and Boutin *et al.* [19] adopted this definition, but there is little variation and $\sigma(S, T)$ is very similar for most models (Appendix I).

The parameter ε_∞ is mathematically the limiting value at $f \to \infty$, but the value in this limit is not established and ε_∞ is treated as a parameter to be determined. It is perhaps the parameter with most variation among the models discussed here. Most models have values ranging from 3 to 6 but with choices ranging from a constant to a function of S and T (details are in Appendix I).

In the following sections, the models will be compared. In Section III, they are compared as a function of frequency and then at 1.4 GHz compared as a function of salinity and temperature. In Section IV, the models will be compared to laboratory measurements of the dielectric constant at 1.4 GHz [15], [17]. The component parts of each model (i.e., relaxation time, static term, conductivity, and high frequency limit) are compared as functions of S and T in Appendix I.

III. Models to Be Compared

The models to be compared are listed in the following in two categories, those composed of a single Debye resonance and those using two resonant terms. Generally, those composed of a single resonance are designed for use near 1.4 GHz and those with two resonances were intended for use at higher microwave frequencies. However, there are exceptions, such as FASTEM [18] and the model of Meissner and Wentz [10], [11], which use two resonances and are applicable at 1.4 GHz, and the model by Guillou *et al.* [9], which includes a single resonance and was intended for use at higher frequencies.

A. Models With a Single Resonance

KS: Klein and Swift [3]: Based on laboratory measurements at 1.43 and 2.65 GHz using a reflection cavity technique by Ho *et al.* [26] and Ho and Hall [27]. The data cover a range of approximately $5 < T < 30$ °C and $4 < S < 35$ psu.

BA: Blanch and Aguasca [16]: Based on laboratory measurements at 1.4 GHz over the range of $0.5 < f < 2.5$ GHz using a transmission line method and with salinity and temperature covering the range $0 < S < 40$ psu and $0 < T < 38$ °C, the later in steps of 7 °C.

GW: Zhou et al. [17]: Based on laboratory measurements at 1.4 GHz using a resonant cavity technique at 1.413 GHz and covering the range $0 < S < 38$ psu and $-1.5 < T < 35$ °C. This is an extension of earlier work, which fit a polynomial to the measurements [28].

BV: Boutin et al. [19]: Uses the functional form in (2) for the static term with $A(T)$ the freshwater value and

$B(T)$ tuned to optimize the retrieval from SMOS measured brightness temperature. The conductivity is as proposed by Stogryn *et al*. [6] and McDougall *et al*. [47], and the relaxation time, $A(T)$ and the high frequency limit are the $S = 0$ values as given by Meissner and Wentz [10], [11]. Tuned to apply at 1.4 GHz and $0 < T < 30$ °C and $32 <$ SSS < 38 psu.

EL: Guillou et al. [9] and Ellison et al. [7]: Based on measurements from 3 to 20 GHz in 0.85-GHz steps and covering $-2 < T < 30$ °C in 1° steps for each of six salinities 23.2, 28.0, 30.024, 35.0, 38.024, and 38.893 psu also with selected measurements in this range at 23.8, 36.5, and 89 GHz. Nominal range for model fit: $3 < f < 20$ GHz, $-2 < T < 30$ °C, and $20 < S < 40$ psu.

B. Models With Two Resonances

MW: Meissner and Wentz [10], [11]: Uses the conductivity given by Stogryn *et al*. [6] and the measurements of Ho *et al.* [26] and Ho and Hall [27] at L- and S-band and Guillou *et al.* [9] at 85 GHz; and the dielectric constant of fresh water is fitted to laboratory measurements in the frequency range 1.7–410 GHz [29], [30], [31], [32]. The relaxation time and other parameters have been tuned to improve the fit to special sensor microwave/imager (SSM/I) and Windsat measured TB especially near 37 GHz [33], [34]. The range of application is $0 < S < 40$ psu, $2 < T < 29$ °C, and frequencies up to 90 GHz.

FM: FASTEM-4: Liu et al. [18]: Input data cover the range $-2 < T < 30$ °C and $0 < S < 35$ psu and $1.4 < f < 410$ GHz. The model parameters are fitted using measurements of the dielectric constant as follows: 1) the measurements at 23.8, 36.5, and 89 GHz for a constant salinity of 38.89 psu and water temperatures of −2 °C, 12 °C, 20 °C, and 30 °C as reported by Ellison *et al*. [7]; 2) the measurements at 1.43 and 2.65 GHz reported by Ho *et al*. [26] and Ho and Hall [27] used in the KS model; 3) measurements at 35 psu at frequencies of 30–105 GHz and at temperatures of −2 °C and $5 < T < 30$ °C in steps of 5 °C as reported by Lamkaouchi *et al*. [35]; and 4) the dielectric constant of fresh water over the frequency range of 1.7–410 GHz reported by Kaatze and Uhlendorf [29], Hasted *et al*. [32], and Ellison *et al*. [36].

EL2: Ellison [8]: Proposed for range: $0 < T < 30$ °C, $0 <$ SSS < 40 psu, and $0 <$ freq < 500 GHz for sea water. This article provides a good review of past work, but the two models provided ("best fit" and "practical") are out of bounds compared to the other models above and it was decided not to include them here. Uses the Stogryn *et al*. [6] model for conductivity.

ST: Stogryn et al. [6]: Based on measurements from 7 to 14 GHz in 1-GHz steps and salinities of 0, 2.09, 3.92, 7.17, 11.2, 15.46, 20.14, 22.47, 31.68, and 35.96 psu and temperatures $0 < T < 30$ °C in 5° steps. Inverts the definition of salinity [25] to obtain conductivity as a function of S and T.

IV. Comparison

A. Dependence on Frequency

The models for the dielectric constant of sea water considered here all have the functional form given by (1) with one or two resonances. Consequently, it is not surprising that the dielectric constant and brightness temperature predicted by models are very similar as a function of frequency. This is illustrated in Figs. 1 and 2. Fig. 1 shows the brightness temperature predicted by the models as a function of frequency at $S = 35$ psu and $T = 20$ °C and nadir incidence angle. The frequency range is $0 < f < 100$ GHz on the top and with better resolution for $f < 5$ GHz on the bottom. Except for model BA above 10 GHz, there is not a great difference at this resolution among the models, although the models with two Debye resonant terms (ST, MW, and FM) tend to predict lower TB for $f > 20$ GHz. Fig. 2 shows the real and imaginary parts of the dielectric constant predicted by the eight models as a function of frequency for $S = 35$ psu and $T = 20$ °C again with full scale in the top panel and with an expanded scale for $f < 5$ GHz in the bottom panel. On the bottom, the BA model (solid green) stands out from the others. At lower frequencies (bottom panel), there are noticeable differences in the real part of the models.

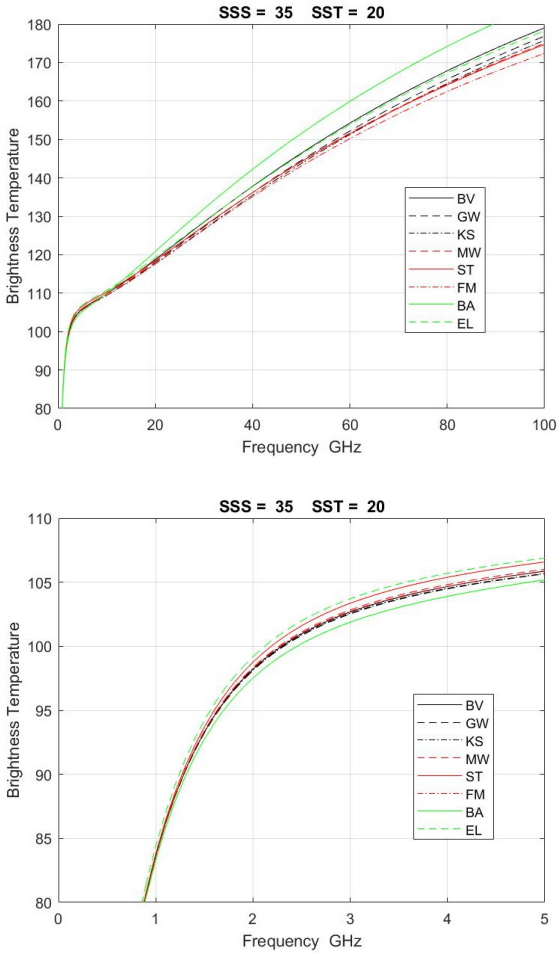

Fig. 1. Brightness temperature predicted by each model versus frequency at nadir with $S = 35$ psu and $T = 20$ °C. (Top) Full scale and (Bottom) with expanded scale to show detail below 5 GHz.

B. Behavior at 1.4 GHz

When the focus is on 1.4 GHz, significant differences are evident in both the brightness temperature predicted by the

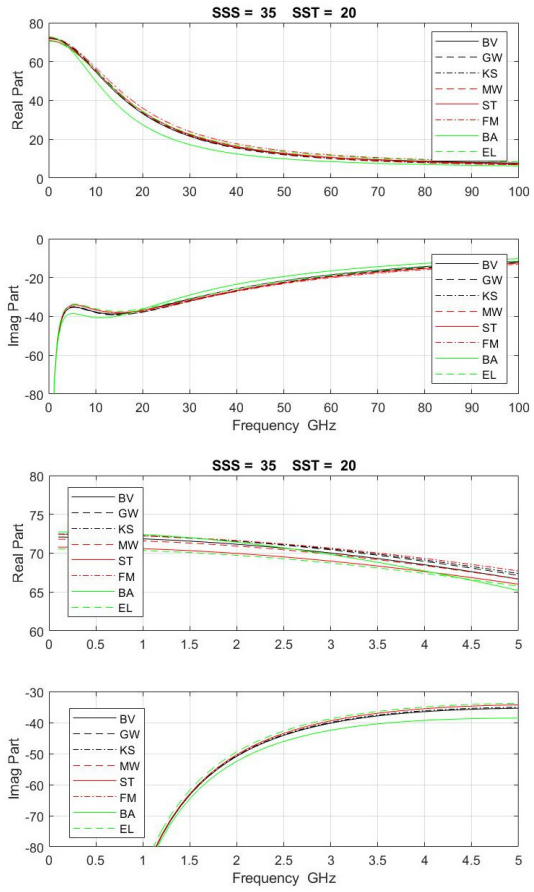

Fig. 2. Each panel shows the real part (top) and imaginary part (bottom) of the models versus frequency. (Top) Full scale and (Bottom) with expanded frequency scale to show detail below 5 GHz.

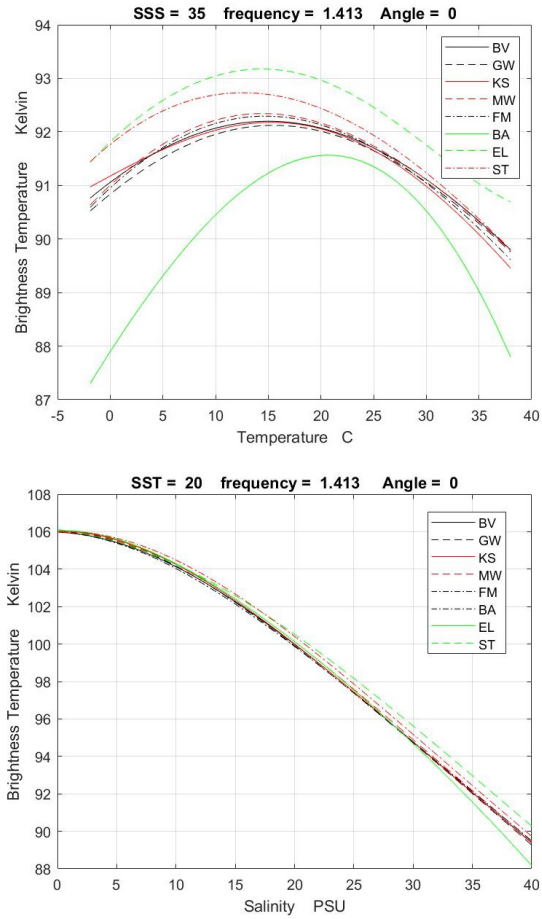

Fig. 3. Brightness temperature at 1.4 GHz for nadir. (Top) As a function of temperature for $S = 35$ psu. (Bottom) As a function of salinity for T = 20 °C.

models and in the dielectric constant itself. This is illustrated in Figs. 3–5.

Fig. 3 shows the brightness temperature, TB, at nadir predicted by each model at 1.4 GHz as a function of temperature (top) for $S = 35$ psu and as a function of salinity (bottom) for $T = 20$ °C. The models differ much more as a function of temperature than as a function of salinity. The salinity dependence is primarily in the conductivity, σ, and static terms, ε_s, which are compared in Appendix I. The conductivity (Appendix I, Fig. 8) is almost identical among the models, and the dependence of ε_s on salinity is similar and approximately linear for most models (Appendix I, Fig. 9, bottom). The relative dependence on S and T shown in Fig. 3 at nadir is independent of polarization and incidence angle. This is illustrated in Appendix II, where the brightness temperature is shown as a function of salinity and temperature at an incidence angle of 40°.

Fig. 4 shows the same information for the dielectric constant. On the top is shown the real and imaginary parts of the dielectric constant at $S = 35$ psu as a function of T and on the bottom is the dielectric constant for the eight models as a function of salinity for $T = 20$ °C. The greatest difference among the models is in the real part of the dielectric constant. The imaginary parts are very similar because $\sigma(S, T)$ is almost identical and the salinity dependence in ε_s is similar among the models (the major exceptions are models EL and BA: see Appendix I).

For remote sensing of salinity, an accuracy of TB of about 0.1 K is required to obtain an accuracy of SSS of 0.2 psu depending on temperature and incidence angle (see [37, Fig. 1]). It is clear from the top panel in Fig. 3 that several of the models (e.g., BA, ST, and EL) stand apart from the others at this level of accuracy. These three models also appear as outliers in Fig. 4 (top panel) for their dependence on temperature (i.e., real part of ST and EL and imaginary part of BA) and in Fig. 4 (bottom panel) for the dependence on salinity of the real part [i.e., ST (red) and EL (green dash) models]. The ST and EL models are based on measurements at higher frequencies and L-band is out of the range of the data used in the model fit. It is not reasonable to expect them to fit at 1.4 GHz. Consequently, these two models will be dropped from further analysis, since the focus is on models representing the dielectric constant at 1.4 GHz. On the other hand, the BA model (green solid) was based on measurements at 1.4 GHz and intended for use in remote sensing of salinity, but Figs. 1–4 suggest something is amiss. This is especially obvious in Fig. 3 (top), which shows the brightness temperature predicted by this model as a function of temperature. It is also clear from the examination of the component parts of the models (Appendix I) that the model for conductivity and the

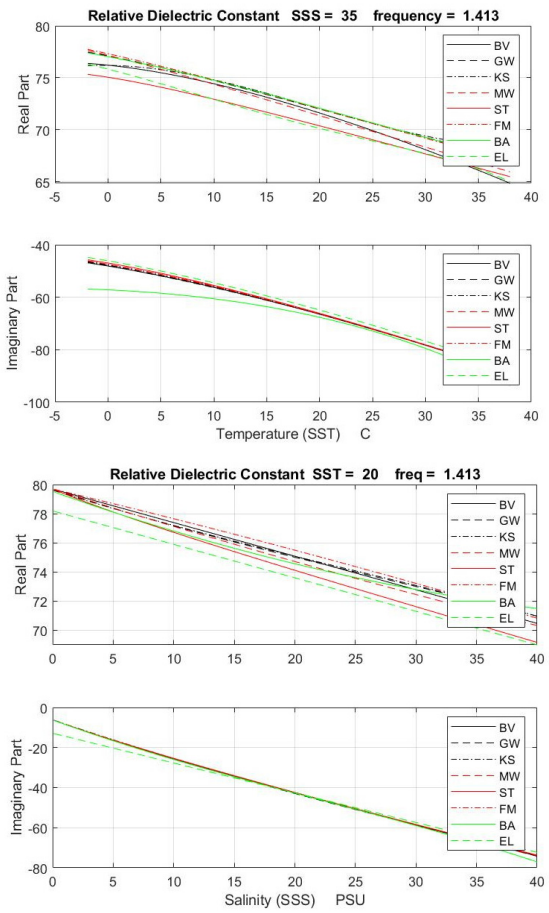

Fig. 4. Comparison at L-band of (Top) real part and (Bottom) imaginary part of the dielectric constant for all models. (Top) Comparison as a function of temperature for $S = 35$ psu. (Bottom) Comparison as a function of salinity for $T = 20$ °C.

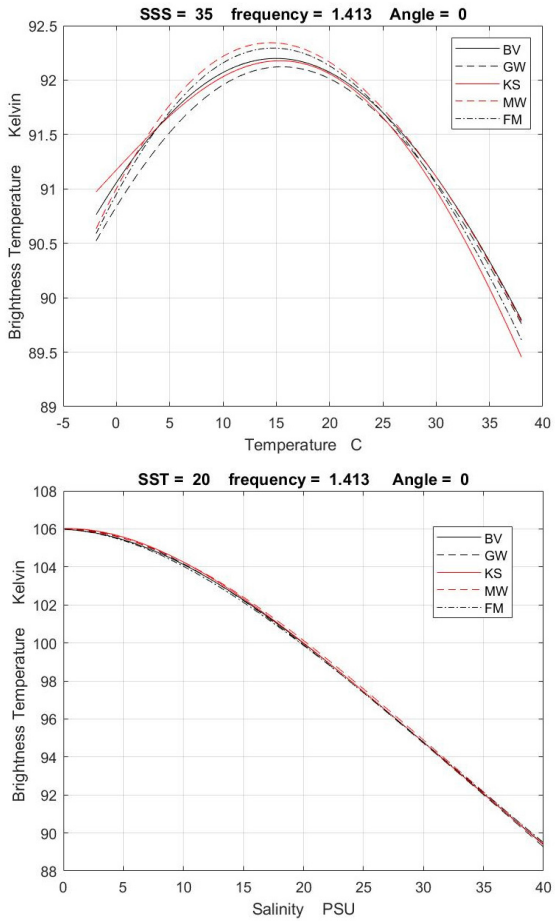

Fig. 5. Comparison at L-band of the brightness temperature predicted at nadir and 1.4 GHz by selected models. (Top) Comparison as a function of temperature for $S = 35$ psu. (Bottom) Comparison as a function of salinity for $T = 20$ °C.

relaxation time associated with the Debye resonance term in this model are unusual. Consequently, this model will also be dropped from further analysis.

Fig. 5 shows the brightness temperature as a function of temperature (top) and salinity (bottom) for the remaining models. Each of these models advertises applicability at L-band. Differences in the dependence on temperature (top) exist that are well in excess of the 0.1-K figure of merit for remote sensing of salinity (see Fig. 16 in Appendix III). The differences are greatest for $T < 20$ °C and smallest near 26 °C. There is much more uniformity in the variation with salinity (Fig. 5, bottom) and the agreement is good for all values of salinity. A figure with expanded resolution for salinity typical of the open ocean, $32 < S < 38$ psu, is shown in Appendix III, where it can be seen that the differences in the dependence on S are on the order 0.1 K.

Brightness temperature is important because it is the parameter measured by satellite remote sensing systems, but it is not necessarily a good indicator of how well the model actually represents the dielectric constant of sea water. This is because the relationship between the dielectric constant and TB is not unique and given TB one cannot uniquely determine both the real and imaginary parts of the dielectric constant [38]. To get a better quantitative assessment of how well these models represent the dielectric constant of sea water at L-band, they will be compared in Section V below with laboratory measurements of the dielectric constant.

V. Comparison With Measurements at 1.4 GHz

While there has been much work on the dielectric constant of pure water and several relatively recent reports of measurements of the dielectric constant of sea water at frequencies associated with remote sensing of SST [6], [7], [9], the measurements at 1.4 GHz are very limited (see [8], [15] for a review). The measurements at 1.4 GHz include the measurements by Ho and Hall [27] used by Klein and Swift [3] with measurements at 2.85 GHz [26] to develop the KS model. More recently, measurements were made at the Universitat Politècnica de Catalunya (UPC) and used to develop the BA model [16]. Unfortunately, the only public record of this work is the article by Blanch and Agusca [16]. The data were not published and the model appears to have issues as discussed above.

The development of radiometers at 1.4 GHz for remote sensing of salinity from satellite missions, such as Aquarius/SAC-D and SMOS, raised the visibility of the need for

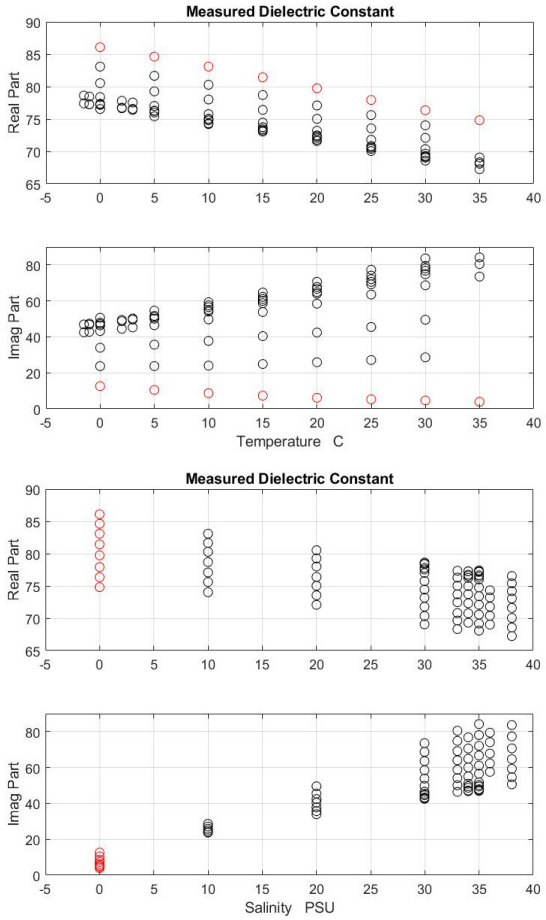

Fig. 6. Measurement of the dielectric constant of sea water as a function of temperature (Top) and salinity (Bottom). The data are from [Lang *et al.*, 2015; Table V] and [17, Tables I–III]. Freshwater ($S = 0$) in red.

accurate measurements of the dielectric constant of sea water at 1.4 GHz [20], [39]. In response, research at The George Washington University was started to make a comprehensive set of measurements at 1.4 GHz [15], [17], [28]. These measurements comprise a wide range of salinity ($0 < S < 38$ psu) and temperature ($-1.5 < T < 30$ °C) and with an emphasis on values likely to be encountered in the open ocean. This is a contemporary set of measurements that used a proven technique (resonant cavity) and takes advantage of modern microwave instrumentation to achieve high accuracy [15]. Measurements were made at fixed salinity as a function of temperature at discrete temperatures and salinity. The data are shown in Fig. 6 as a function of temperature (top) and as a function of salinity (bottom). The spread in the data in the top panel represents the dependence of the dielectric on salinity at each of the temperatures at which measurements were made and in the bottom panel represents the dependence on temperature for each salinity used in the measurements. The measured values of dielectric constant are in [15, Table V] and [17, Tables I–III]. The complete dataset is available online at [40].

Rather than comparing the models for the dielectric constant point by point with the data, an alternative that yields a better visualization of the comparison is to compare with an interpolation function that represents this data. This introduces additional error and the accuracy of the fit, but it permits smooth curves that allow one to see patterns in how the models compare with the data as a function of temperature and salinity. The obvious interpolation function for this data is the model developed by the GWU team [17], which is a best fit to the data. This is the model GW listed in Section III and discussed above. It is a fit to the data using the functional form of (1) with a polynomial in S and T for the unknowns, ε_s and σ. The relaxation time was assumed to be the same as for freshwater and fitted to the measurements (red circles in Fig. 6). The high-frequency limit was set at 4.9 as recommended by Klein and Swift [3]. Fortunately, a careful analysis of the accuracy of the measurements in 2016 was documented [15]. It is assumed that this is representative although improvements were made leading to the measurements reported in [17]. In the case of the real part, the standard deviation (STD) of the total measurement error is 0.23, and for the imaginary part, the STD of the total measurement error is 0.26. The STD of the difference between the GW model and the data at each point is 0.11 for the real part and 0.29 for the imaginary part. Assuming that measurement and representation errors are independent, the net error for representation (square root of the sum of the squares) is 0.25 for the real part and 0.36 for the imaginary part. Differences between a particular model under consideration here and the GW interpolation that are within one STD (i.e., ± 0.25 for the real part) will be used here to suggest good agreement with the data. The differences are reported in Fig. 7.

Fig. 7 shows the difference between GW and the models, BV, KS, MW, and FM as a function of temperature for SSS = 35 psu (top) and as a function of salinity with SST = 20 °C (bottom). The green dashed horizontal lines indicate the STD of the combined error of the interpolation (fit of GW to the data) and the data itself. In general, the fits are better for the imaginary parts than for the real parts and better as a function of salinity than as a function of temperature. As mentioned above, this is a consequence of a great deal of similarity in how the salinity dependence is included among the models. In particular, the BV, MW, and FM model all use the Stogryn [6] inversion of the definition of salinity or equivalent (see [47]). The GW and KS versions, which were determined independently using polynomial fits to their respective data, are almost identical (Appendix I). The largest variation among the models is in the behavior of the real part as a function of temperature. This reflects the differences in how the models included T in the parameterization of the static term, ε_s.

The best fit of all appears with KS, which also happens to be the other model based on laboratory measurements at L-band. The KS model is consistently within the error bounds in all four panels except for the real part at temperatures below 5 °C and above 30 °C (top panel), which are temperatures out of the range of the measurements used in developing the KS model. At temperatures and salinities in the range of $20 < T < 30$ °C and $30 < S < 40$ psu, the FM model is

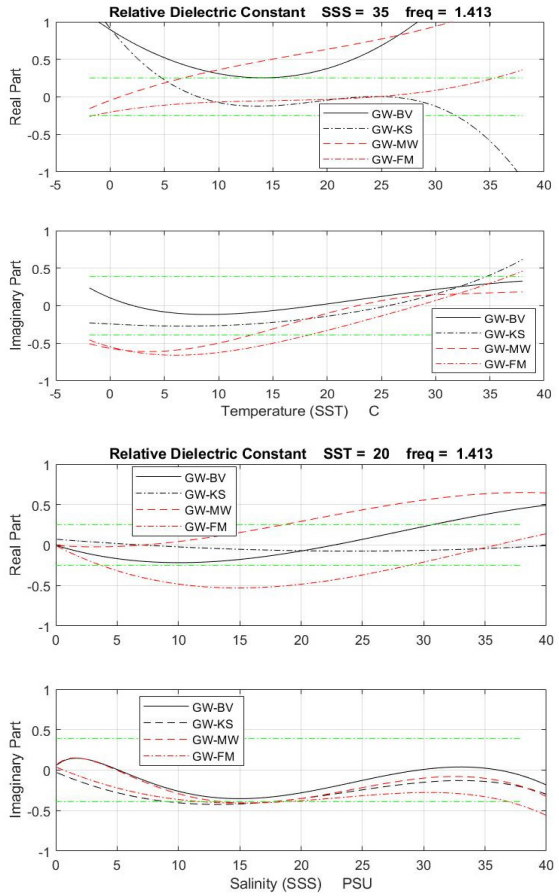

Fig. 7. Comparison of models for the dielectric constant with the GW model as a function of (Top) temperature and (Bottom) salinity.

also consistently within the error bounds. This model used in its development the same measurements at 1.4 GHz by Ho *et al*. [26] as used for developing the KS model.

VI. Discussion

Perhaps, it is not surprising that the two models based on laboratory measurements of the dielectric constant, KS and GW, should be close. The two sets of measurements are completely independent and so are the model fits, although the two models use the same functional form [(1)] and the same high-frequency limit, $\varepsilon_\infty = 4.9$ (Appendix I). The agreement of these two models is a positive indication for both the quality of the measurements and the quality of the data fits (but see [15] for more information about the Ho and Hall [27] data).

In the two models, BV and MW, parameters were tuned to optimize the science retrieval algorithm by choosing the model parameters to minimize the differences between radiative transfer simulations of the brightness temperature and the TB actually observed by the satellite. These two models are close to the measurements but diverge in some significant respects. This is particularly evident in the temperature dependence of the real part (Fig. 7, top). The BV model was tuned to optimize the retrieval of salinity from SMOS observations of brightness temperature at 1.4 GHz. The tuning was done on the temperature dependence of the static term [term $A(T)$ in (2)], which is strongly coupled to the real part. The MW model is a double Debye resonance model intended to cover a large range of higher frequencies and the tuning was done to fit the satellite observations from Windsat and SSM/I in this higher range and particularly near 37 GHz. The FM model, which is also a double resonance model intended for use over an extended range of frequency, uses data at several frequencies from several sources. The fit at 1.4 GHz is mixed. It fits the real part well as a function of temperature at 35 psu (Fig. 7, top panel) but not as well for $S < 30$ (Fig. 7, bottom panel). The imaginary part agrees with the measurements well for 20 °C and above (Fig. 7, bottom panel) but not as well at lower temperatures.

Three of the models in Fig. 7 have been used in remote sensing of salinity: KS and BV have been used in SMOS retrievals and MW was used for Aquarius and is now used for retrieving salinity from soil moisture active passive (SMAP). In addition, a combination of the MW and KS model has been used in the combined active passive (CAP) algorithm for retrievals from Aquarius and SMAP [41]. These models have been used quite successfully to retrieve salinity. However, this success does not guarantee that they are a good representation of the dielectric constant of sea water. For example, the MW model was used quite successfully to retrieve salinity from both Aquarius and SMAP [42], but this does not mean it is the best representation of the dielectric constant of sea water. On the contrary, except for cold temperatures, KS appears to be a better fit to the dielectric constant at 1.4 GHz.

The contradiction lies in the realities of the retrieval algorithm. There are many inputs to the retrieval algorithm each with associated uncertainty that require adjustments. For example, the algorithm starts with the best available models for the sensor antenna and for propagation from the surface to the sensor and makes adjustment to improve the retrieval of the science product via iteration with surface truth. This process can hide deficiencies in models adopted as "known" input. For example, an SST-dependent bias was noticed in one of the early versions (Version 3.0) of the retrieval of SSS from Aquarius [43]. This was corrected with an adjustment to the surface emissivity used in the retrieval algorithm (see [42]). The result was a retrieval in excellent agreement with surface truth and little SST dependent bias, but the source of the error was not identified. It was later shown that switching models for the dielectric constant to KS reduced this bias [43]. The choice of models may well be the source of this error, but it was not necessary to make a change because of adjustments made in the retrieval algorithm.

The example above is a reminder that the success of Aquarius, SMAP, and SMOS in retrieving accurate values of SSS does not automatically assure that the model used in the algorithm for the dielectric constant is accurate. On the other hand, the more accurate the model, the more likely the retrieval is to be successful and the more potential there is for improvement of the retrieved SSS. For example, suppose one had a perfect model for the dielectric constant and encountered a temperature-dependent bias in the retrieval as occurred with Aquarius. In this case, having the correct model would

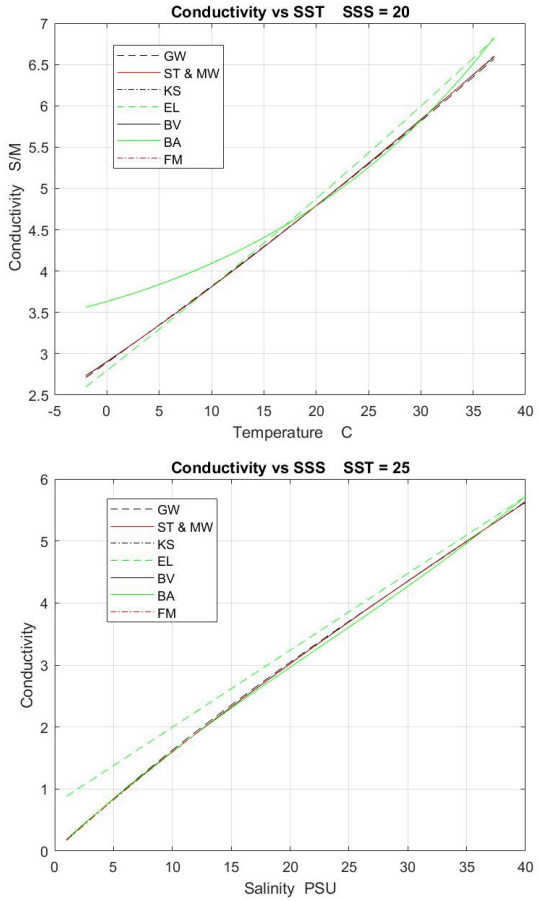

Fig. 8. Conductivity as a function of temperature and salinity. (Top) Conductivity at $S = 20$ psu as a function of temperature. (Bottom) Conductivity at $T = 25$ °C as a function of salinity. GW—black dash; ST and MW—red; KS—black dashed dotted; EL—green dash; BV—black; BA—green; and FM—red dashed dotted.

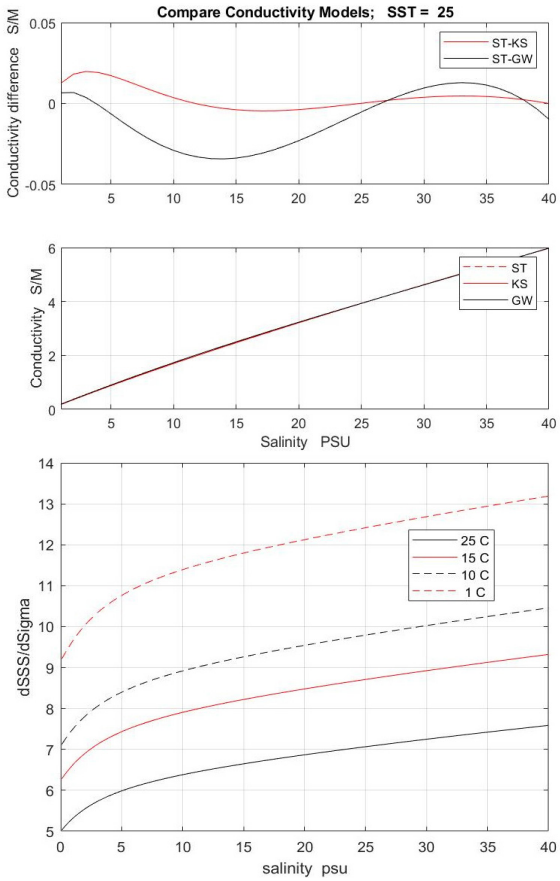

Fig. 9. Comparison of GW and KS conductivity, $\sigma(S, T)$ with the Stogryn, ST, model. (Top): Difference. (Middle): Comparison. (Bottom): Slope dS/dσ in PSU/(S/m) for several values of SST.

eliminate this part of the algorithm as a potential source of error and would direct the research for the root cause elsewhere. The result likely would be a better understanding of errors in the retrieval algorithm itself.

The search for a model for the dielectric constant of sea water at 1.4 GHz accurate enough to promote improvements in the retrieval of is not yet complete. There are at least two challenges. One is that making measurements that are consistent with an accuracy of the salinity product of better than 0.2 psu is very hard. For example, at nadir, an accuracy of 0.2 psu corresponds to radiometric accuracy of 0. 1 K for a measurement at 1.4 GHz (see [37, Fig. 4]). Assuming equal error, Δ, in the real and imaginary parts of the dielectric constant, an accuracy of about $\Delta = 0.25\%$ in the measurement of the dielectric constant is required (at 35 psu and 25 °C) to have an error of less than 0.1 K in TB. The current measurement accuracy of the GW measurements at this temperature and salinity is about 0.35% [15]. So, there is yet a need for improvement, and if the goal is eventually to achieve 0.1 psu, even more progress is needed. The second issue is the possibility that remote sensing of salinity in the future will become a multispectral process. The peak sensitivity to SSS lies below 1.4 GHz [37], and research has been reported suggesting that a wideband radiometer operating in the range 0.5–2.0 GHz could enhance the accuracy of the retrieval of SSS especially in cold water by including frequencies closer to the peak [44], [45]. Simply applying existing models to these frequencies does not guarantee their validity, and new measurements will be needed to determine the coefficients of models suitable for this range of frequencies with the accuracy needed to retrieve SSS. Work to address this problem has already begun [46].

In the meantime, a problem with many models is the use of the models outside of their range of validity. There are no physical restrictions, which prevent using any of these models at any frequency, salinity, or temperature, but all the models discussed here are based on measurements of a finite range in S and T and use mathematical functions (usually polynomials) to fit the unknown parameters to the data in this range. The fits are unconstrained outside of the range of the data. This is evident in the case of the KS model. As can be seen in Fig. 7 (top panel), the real part diverges strongly from the measurements for high ($T > 30$ °C) and low temperatures ($T < 5$ °C). Using this model for retrievals at low temperature results in large errors, which have been well documented [43]. Another obvious example is the EL and ST models, which were built on measurements at frequency above L-band (minimum frequency of 3 and 7 GHz, respectively).

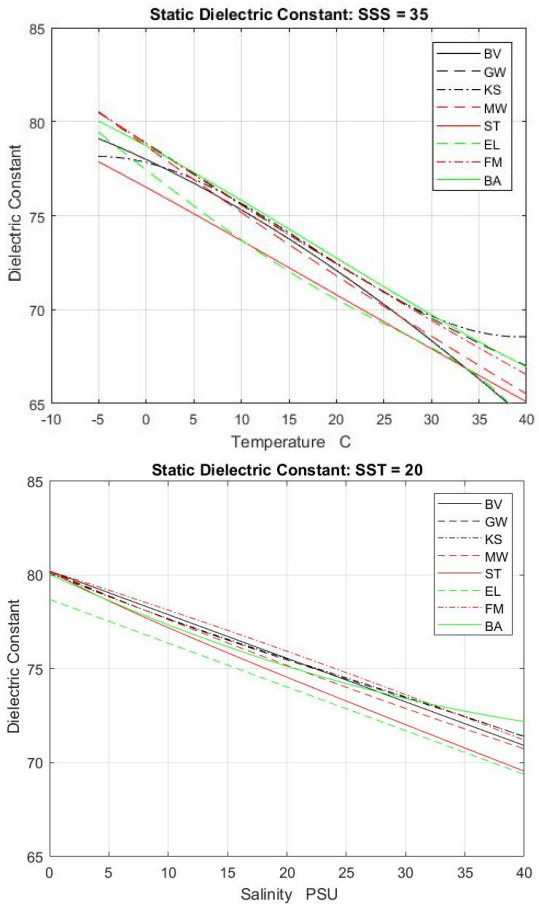

Fig. 10. Static term as a function of (Top) temperature for $S = 35$ psu (Bottom) and as a function of salinity $T = 20$ °C.

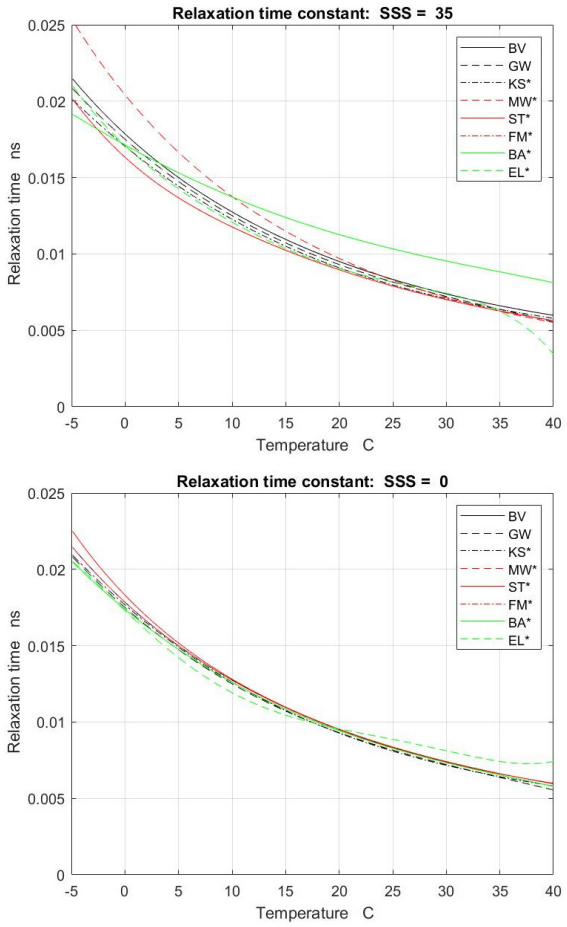

Fig. 11. First relaxation time as a function of temperature for (Top) freshwater and (Bottom) for $S = 35$ psu.

Mathematically, there is no problem applying them at 1.4 GHz. However, they are not representative of the brightness temperature of the ocean surface at 1.4 GHz as the examples in Figs. 3 and 4 show.

APPENDIX I

All the models discussed in this article have the form of (1), which has several common parameters that are determined by fitting the model to observation of the real world. In this Appendix, the parameters, conductivity, static dielectric constant, the relaxation time of the first resonance, and the high-frequency limit will be compared.

A. Conductivity, $\sigma(S, T)$

With the establishment of the practical salinity scale [25], the definition of salinity was tied to conductivity. Salinity was defined as a ratio of measured conductivity to that of a standard solution at a 15 °C and experiments provided conversions for temperature and pressure [25, eq. (9)]. Stogryn *et al.* [6] reported an inversion of this definition to produce an expression for $\sigma(S, T)$, which is equivalent to a more recent version [47]. Most models adhere closely to this definition. This is illustrated in Fig. 8, which shows the conductivity, $\sigma(S, T)$, on top as a function of T for $S = 35$ psu and on the bottom as a function of S for $T = 20$ °C for each of the models. With the exception of EL (green dash) and BA (green), there is very good agreement among the models. The models ST, MW, and BV use the inversion from the definition for conductivity. The KS and GW models use a polynomial in S and T to represent $\sigma(S, T)$ with coefficients that are determined from their respective measurements of the dielectric constant (i.e., see [26], [27] in the case of KS and [15], [17] in the case of GW). The FM model uses the KS expression for conductivity. The two polynomial fits are in very good agreement with the definition. This is illustrated in Fig. 9, which shows the KS and GW expressions for conductivity together with the expression derived by Stogryn *et al.* [6] and used in ST as a function of salinity in the top two panels. On the top, the differences ST–KS and ST–GW are shown to make the difference more visible. To put these differences in context, the change in salinity with conductivity, $dS/d\sigma$, is plotted in the bottom panel for $T = 25$ °C. A difference of about 0.03 S/M corresponds to a salinity difference of about 0.2 psu at 35 psu and this temperature (25 °C) and less with a decrease in salinity. Using the goal of contemporary remote sensing of SSS from space of an accuracy of 0.2 psu as

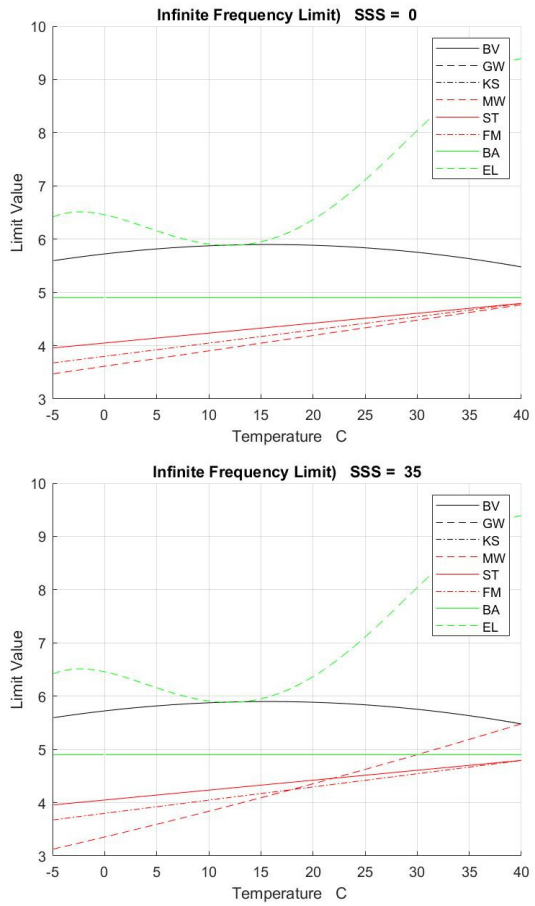

Fig. 12. High-frequency limit. As a function of temperature for (Top) $S = 0$ and (Bottom) $S = 35$. Only MW depends on salinity. GW, BA, and KS all use the constant value = 4.9.

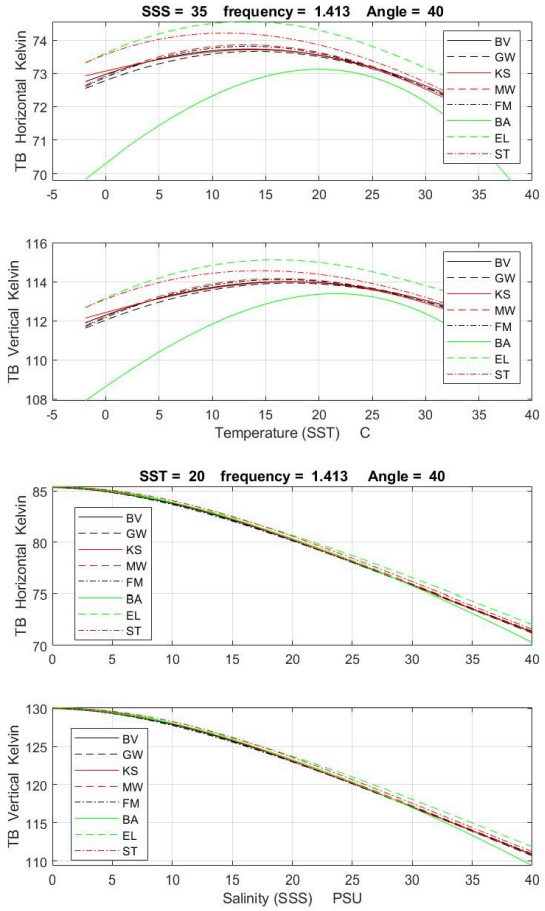

Fig. 13. Brightness temperature at 1.4 GHz and 40° incidence angle as a function of temperature with (Top) $S = 35$ psu and as a function of salinity with (Bottom) $T = 20$ °C. In each panel, horizontal polarization is on the top and vertical polarization is on the bottom.

a metric, the models for conductivity determined by model fits to measurements are in good agreement with the expression obtained by inverting the definition of salinity (which is a reassuring result for both measurements and inversion of the definition).

B. Static Term, ε_s

The static term, ε_s, is shown in Fig. 10 as a function of T for $S = 35$ psu (top) and as a function of S for $T = 20$ °C on the bottom. The model, EL, is clearly an outlier and does not converge to the same value for freshwater ($S = 0$, bottom panel) as all the other models. Its temperature dependence at $S = 0$ (not shown here) is also much different than that of the other models. The variation with both salinity and temperature is approximately linear over the range shown in Fig. 10, although the BA model (green solid) has a noticeable curvature in its dependence on salinity (bottom panel). The KS model is an outlier at very cold and very warm temperatures (dashed-dotted curve, top panel), but the KS model was based on measurements for 5 °C $< T <$ 30 °C, and there is no reason to expect the polynomials fitted to the data to extrapolate well to temperatures out of this range.

C. Relaxation Time, τ

Comparison is made here only for the relaxation time, τ_1, of the first Debye resonance. The resonant frequency, τ_2, associated with the second resonance is around 100 GHz and this term is not important for application near L-band. The first relaxation time, τ_1, for all the models is close to the freshwater value with a weak or no dependence on salinity. This is illustrated in Fig. 11, in which τ_1 is plotted as a function of temperature for freshwater ($S = 0$) on top and for SSS = 35 psu on the bottom. In the case of fresh water, all the models except for BA (green dash) are close together and have a similar dependence on temperature. The resonant frequency at 20 °C is about 17 GHz and varies with temperature increasing to about 30 GHz at 40 °C and decreasing to about 10 GHz at 0 °C. All the models assume a weak dependence on salinity except for BV and GW, in which τ is independent of S. This can be seen by comparing the curves in the panel on the top ($S = 0$) with those in the bottom panel of Fig. 11, which shows τ_1 as a function of temperature for $S = 35$ psu. The dependence on salinity in those models that include a dependence on SSS is very weak for $T > 20$ °C and increases at lower temperatures as can be seen in the spread of the curves in the bottom panel of Fig. 11.

D. High-Frequency Limit, ε_∞

The high-frequency limit, ε_∞, is shown in Fig. 12 as a function of SST for freshwater ($S = 0$) on the top and for sea

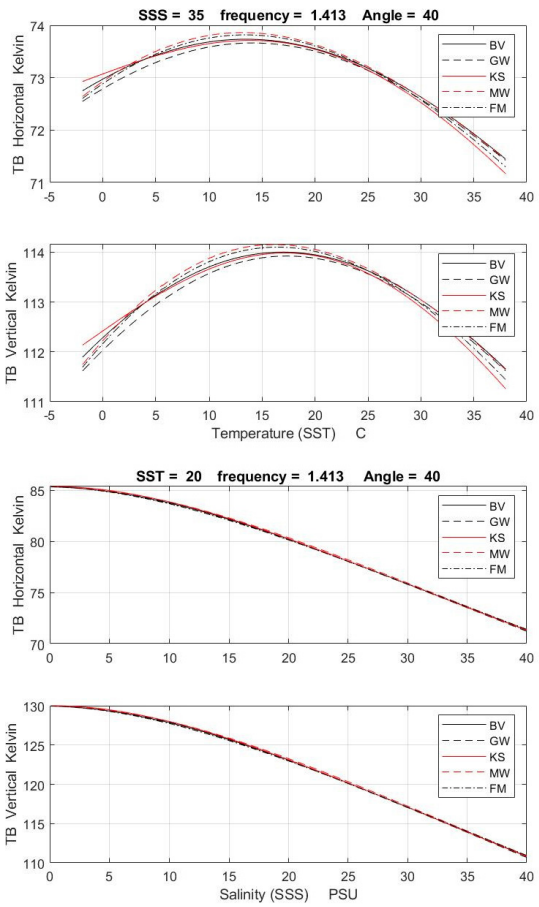

Fig. 14. Same as Fig. 13 but with models ST, EL, and BA removed to permit enhanced resolution. Brightness temperature at 1.4 GHz and 40° incidence angle as a function of temperature (Top) with $S = 35$ psu and as a function of salinity with (Bottom) $T = 20$ °C. In each panel, horizontal polarization is on the top and vertical polarization is on the bottom.

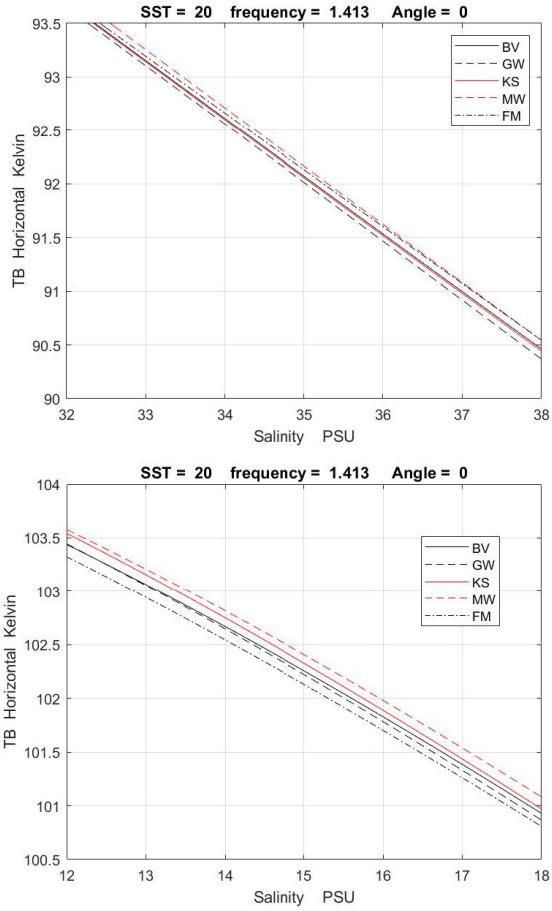

Fig. 15. Dependence of brightness temperature, TB, at 1.4 GHz and nadir incidence as a function of salinity with expanded scale to show differences. The differences among the models depend on the value of salinity: (Top) for $32 < S < 38$ and (Bottom) for $12 < S < 18$. The vertical and horizontal scales have the same resolution in each panel to facilitate comparison.

water (SSS = 35 psu) on the bottom. Only the MW model (red dash) includes a dependence on salinity. In the models using a single Debye term (KS, GW, BA, BV, and EL), $\varepsilon_\infty \equiv \varepsilon_1$. Three models, KS, GW, and BA, assume a constant value, $\varepsilon_\infty = 4.9$, which was suggested by Klein and Swift [3]. With the exception of EL (green dash), all of other models have values close to this but with a small dependence on temperature.

There appears to be no consensus as to what the dielectric constant should be at very high frequency, and this parameter plays the role of a free parameter to be adjusted to improve the fit. The choice made by model builders appears to depend on the functional form (one or two Debye terms) chosen for the dielectric constant. For example, the red curves correspond to models (ST, MW, and FM) that employ two Debye resonance. On the other hand, the constant, 4.9, and black curve (BV) correspond to models using a single Debye resonance. A similar partition depending on the number of Debye terms is reported by Liebe et al [24] in the case of freshwater. The values for ε_∞ reported by Liebe are consistent with those shown in Fig. 12 (top) with the exception of EL (green dash), which is an outlier.

When frequency $f \ll 1.4$ GHz, the infinite frequency limit, ε_∞, has negligible effect on the dielectric constant. In this case, $\omega\tau_2 < \omega\tau_1 \ll 1$, and both ε_∞ and ε_1 cancel themselves in (1). The effect of ε_∞ is also small at 1.4 GHz, although not necessarily negligible. For example, using the KS model as an example and varying ε_∞ over the range $3.5 < \varepsilon_\infty < 6$, which covers the range of values appearing in the models discussed here (except for EL), then the change in the imaginary part (where the change is greatest) is about 0.3%. This is small, but this is comparable to the accuracy needed to retrieve salinity at an accuracy of 0.2 psu (see Section VI).

APPENDIX II

Fig. 13 shows the brightness temperature predicted at 1.4 GHz by each of the models for the dielectric constant at 40° incidence angle. The brightness temperature at S = 35 psu is shown as a function of temperature on the top and TB is shown at $T = 20$°C as a function of salinity on the bottom. Horizontal polarization is on the top and vertical polarization on the bottom in both panels. Fig. 14 shows the same as

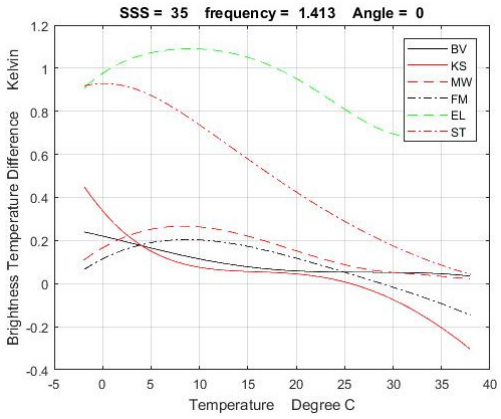

Fig. 16. Difference in brightness temperature at 1.4 GHz between each model and the GW model ($TB_{model} - TB_{GW}$) as a function of temperature for nadir incidence and SSS = 35 psu.

Fig. 13 but with models ST, EL, and BA removed to permit enhanced resolution.

Appendix III

Figs. 15 and 16 in this Appendix provide additional detail for the comparison of the models shown in Figs. 3 and 5. The two panels in Fig. 15 are the same as Fig. 5 (bottom) in the main text but with an expanded scale to show the differences among the models in more detail. Each figure shows the brightness temperature predicted by the selected models at 1.4 GHz and $T = 20$ °C as a function of salinity. The panel on top is the same as Fig. 5 but limited to $32 < S < 38$ psu and the panel on the bottom is the same as Fig. 5 but limited to $12 < S < 18$ psu. The vertical scale resolution is the same in each panel in Fig. 15 to facilitate comparison. Fig. 16 provides additional information on the dependence of the models on SST (see top panel of Fig. 5). Fig. 16 shows the difference in brightness temperature between each model and the GW model. The ST and EL models shown in Fig. 3 have been included in this comparison for completeness. To put the difference in TB in context, the sensitivity of TB to a change in SSS at nadir is about 0.5 K/psu at SST = 20 °C and SSS = 35 psu [37], [44]. Thus, a difference of 0.1 K corresponds to a change of about 0.2 psu, which is the goal of contemporary remote sensing from space [12], [14].

References

[1] K. R. Carver, C. Elachi, and F. T. Ulaby, "Microwave remote sensing from space," *Proc. IEEE*, vol. 73, no. 6, pp. 970–996, Jun. 1985.

[2] C. T. Swift and R. E. Mcintosh, "Considerations for microwave remote sensing of ocean-surface salinity," *IEEE Trans. Geosci. Remote Sens.*, vol. GRS-21, no. 4, pp. 480–491, Oct. 1983.

[3] L. Klein and C. Swift, "An improved model for the dielectric constant of sea water at microwave frequencies," *IEEE J. Ocean. Eng.*, vol. OE-2, no. 1, pp. 104–111, Jan. 1977.

[4] P. J. W. Debye, *Polar Molecules*. Dover, IL, USA: Dover, 1929.

[5] R. Somaraju and J. Trumpf, "Frequency, temperature and salinity variation of the permittivity of seawater," *IEEE Trans. Antennas Propag.*, vol. 54, no. 11, pp. 3441–3448, Nov. 2006.

[6] A. P. Stogryn, H. T. Bull, K. Rubayi, and S. Iravanchy, "The microwave permittivity of sea and fresh water," Gen. Corp Aerojet, Azusa, CA, USA, Tech. Rep., 1995.

[7] W. Ellison *et al.*, "New permittivity measurements of seawater," *Radio Sci.*, vol. 33, no. 3, pp. 639–648, May/Jun. 1998, doi: 10.1029/97RS02223.

[8] W. Ellison, "Fresh and sea water, section 5.2," in *Thermal Microwave Radiation: Applications for Remote Sensing* (IET Electromagnetic Wave Series), vol. 52, Matzler, Ed. London, U.K.: Institution of Engineering and Technology, 2006.

[9] C. Guillou *et al.*, "Impact of new permittivity measurements on sea surface emissivity modeling in microwaves," *Radio Sci.*, vol. 33, no. 3, pp. 649–667, May 1998, doi: 10.1029/97rs02744.

[10] T. Meissner and F. J. Wentz, "The complex dielectric constant of pure and sea water from microwave satellite observations," *IEEE Trans. Geosci. Remote Sens.*, vol. 42, no. 9, pp. 1836–1849, Sep. 2004.

[11] T. Meissner and F. J. Wentz, "The emissivity of the ocean surface between 6 and 90 GHz over a large range of wind speeds and earth incidence angles," *IEEE Trans. Geosci. Remote Sens.*, vol. 50, no. 8, pp. 3004–3026, Aug. 2012.

[12] S. Mecklenburg *et al.*, "ESA's soil moisture and oceansalinity mission: Mission performance and operations," *IEEE Trans. Geosci. Remote Sens.*, vol. 50, no. 5, pp. 1354–1366, May 2012, doi: 10.1109/TGRS.2012.2187666.

[13] Y. H. Kerr *et al.*, "The SMOS mission: New tool for monitoring key elements of the global water cycle," *Proc. IEEE*, vol. 98, no. 5, pp. 666–687, May 2010.

[14] D. M. L. Vine, G. S. E. Lagerloef, F. R. Colomb, S. H. Yueh, and F. A. Pellerano, "Aquarius: An instrument to monitor sea surface salinity from space," *IEEE Trans. Geosci. Remote Sens.*, vol. 45, no. 7, pp. 2040–2050, Jul. 2007.

[15] R. Lang, Y. Zhou, C. Utku, and D. L. Vine, "Accurate measurements of the dielectric constant of seawater at L band," *Radio Sci.*, vol. 51, no. 1, pp. 2–24, Jan. 2016, doi: 10.1002/2015RS005776.

[16] S. Blanch and A. Aguasca, "Seawater dielectric permittivity model from measurements at L band," in *Proc. IEEE Int. Geosci. Remote Sens. Symp. (IGARSS)*, vol. 2, Sep. 2004, pp. 1362–1365, doi: 10.1109/IGARSS.2004.1368671.

[17] Y. Zhou, R. H. Lang, E. P. Dinnat, and D. M. L. Vine, "Seawater Debye model function at L-band and its impact on salinity retrieval from aquarius satellite data," *IEEE Trans. Geosci. Remote Sens.*, vol. 59, no. 10, pp. 8103–8116, Oct. 2021, doi: 10.1109/TGRS.2020.3045771.

[18] Q. Liu, F. Weng, and S. J. English, "An improved fast microwave water emissivity model," *IEEE Trans. Geosci. Remote Sens.*, vol. 49, no. 4, pp. 1238–1250, Apr. 2011, doi: 10.1109/TGRS.2010.2064779.

[19] J. Boutin *et al.*, "Correcting sea surface temperature spurious effects in salinity retrieved from spaceborne L-band radiometer measurements," *IEEE Trans. Geosci. Remote Sens.*, vol. 59, no. 9, pp. 7256–7269, Sep. 2021 doi: 10.1109/TGRS.2020.3030488.

[20] E. P. Dinnat, J. Boutin, G. Caudal, J. Etcheto, and P. Waldteufel, "Influence of sea surface emissivity model parameters at L-band for the estimation of salinity," *Int. J. Remote Sens.*, vol. 23, no. 23, pp. 5117–5122, Jan. 2002, doi: 10.1080/01431160210163119.

[21] C. J. F. Böttcher and P. Bordewijk, "Theory of electric polarization," in *Dielectrics in Time-Dependent Fields*. Amsterdam, The Netherlands: Elsevier, 1978.

[22] P. W. Rosenkranz, "A model for the complex dielectric constant of supercooled liquid water at microwave frequencies," *IEEE Trans. Geosci. Remote Sens.*, vol. 53, no. 3, pp. 1387–1393, Mar. 2015.

[23] A. Stogryn, "Equations for calculating the dielectric constant of saline water (Correspondence)," *IEEE Trans. Microw. Theory Techn.*, vol. MTT-19, no. 8, pp. 733–736, Aug. 1971.

[24] H. J. Liebe, G. A. Hufford, and T. Manabe, "A model for the complex permittivity of water at frequencies below 1 THz," *Int. J. Infr. Millim. Waves*, vol. 12, no. 7, pp. 659–675, Jul. 1991.

[25] E. Lewis, "The practical salinity scale 1978 and its antecedents," *IEEE J. Ocean. Eng.*, vol. OE-5, no. 1, pp. 3–8, Jan. 1980.

[26] W. W. Ho, A. W. Love, and M. J. VanMelle, "Measurements of the dielectric properties of sea water at 1.43 GHz," NASA, Washington, DC, USA, Tech. Rep. CR-2458, 1974.

[27] W. Ho and W. F. Hall, "Measurements of the dielectric properties of seawater and NaCl solutions at 2.65 GHz," *J. Geophys. Res.*, vol. 78, no. 27, pp. 6301–6315, Sep. 1973, doi: 10.1029/JC078i027p06301.

[28] R. Lang, Y. Zhou, E. Dinnat, and D. L. Vine, "The dielectric constant model function and implications for remote sensing of salinity," in *Proc. IEEE Int. Geosci. Remote Sens. Symp. (IGARSS)*, Jul. 2017, pp. 3572–3574.

[29] U. Kaatze and V. Uhlendorf, "The dielectric properties of water at microwave frequencies," *Zeitschrift Für Physikalische Chem.*, vol. 126, no. 2, pp. 151–165, Feb. 1981.

[30] D. Bertolini, M. Cassettari, and G. Salvetti, "The dielectric relaxation time of supercooled water," *J. Chem. Phys.*, vol. 76, no. 6, pp. 3285–3290, Mar. 1982, doi: 10.1063/1.443323.

[31] J. Barthel, K. Bachhuber, R. Buchner, H. Hetzenauer, and M. Kleebauer, "A computer-controlled system of transmission lines for the determination of the complex permittivity of lossy liquids between 8.5 and 90 GHz," *Berichte der Bunsengesellschaft Für Physikalische Chem.*, vol. 95, no. 8, pp. 853–859, Aug. 1991, doi: 10.1002/bbpc.19910950802.

[32] J. B. Hasted, S. K. Husain, F. A. M. Frescura, and J. R. Birch, "The temperature variation of the near millimetre wavelength optical constants of water," *Infr. Phys.*, vol. 27, no. 1, pp. 11–15, Jan. 1987.

[33] F. J. Wentz, "A well calibrated ocean algorithm for special sensor microwave/imager," *J. Geophys. Res.*, vol. 102, pp. 8703–8718, Apr. 1997.

[34] F. J. Wentz and T. Meissner. (2000). *AMSR Ocean Algorithm, Version 2, Report Number 121599A-1, Remote Sensing Systems*. Santa Rosa, CA, USA, [Online]. Available: https://images.remss.com/papers/rsstech/2000_121599A-1_Wentz_AMSR_Ocean_Algorithm_ATBD_Version2.pdf

[35] K. Lamkaouchi, A. Balana, G. Delbos, and W. J. Ellison, "Permittivity measurements of lossy liquids in the frequency range 20–110 GHz," *Meas. Sci. Technol.*, vol. 14, no. 4, pp. 1–7, Apr. 2003.

[36] W. J. Ellison *et al.*, "A comparison of ocean emissivity models using the advanced microwave sounding unit, the special sensor microwave imager, the TRMM microwave imager, and airborne radiometer observations," *J. Geophys. Res., Atmos.*, vol. 108, no. 21, p. 4663, Nov. 2003, doi: 10.1029/2002JD003213.

[37] D. M. L. Vine and E. P. Dinnat, "The multifrequency future for remote sensing of sea surface salinity from space," *Remote Sens.*, vol. 12, no. 9, p. 1381, Apr. 2020, doi: 10.3390/rs12091381.

[38] P. Waldteufel, J. L. Vergely, and C. Cot, "A modified cardioid model for processing multiangular radiometric observations," *IEEE Trans. Geosci. Remote Sens.*, vol. 42, no. 5, pp. 1059–1063, May 2004.

[39] E. P. Dinnat, J. Boutin, G. Caudal, and J. Etcheto, "Issues concerning the sea emissivity modeling at L band for retrieving surface salinity," *Radio Sci.*, vol. 38, no. 4, pp. 1–25, Aug. 2003, doi: 10.1029/2002RS002637.

[40] GWU. (2021). *The Following Website is Located on the NASA/JPL PODAAC; See NASA Salinity Dielectric Constant Data and Documentation*. [Online]. Available: https://podaac.jpl.nasa.gov/Aquarius?sections=data, and https://podaac-tools.jpl.nasa.gov/drive/files/allData/aquarius/docs/Dielectric_Constant/GW2019_dielectric_constant_measurements.h5

[41] S. Yueh, W. Tang, A. Fore, A. Hayashi, Y. T. Song, and G. Lagerloef, "Aquarius geophysical model function and combined active passive algorithm for ocean surface salinity and wind retrieval," *J. Geophys. Res., Oceans*, vol. 119, no. 8, pp. 5360–5379, Aug. 2014, doi: 10.1002/2014JC009939.

[42] T. Meissner, F. J. Wentz, and L. Vine, "The salinity retrieval algorithms for the NASA aquarius version 5 and SMAP version 3 releases," *Remote Sens.*, vol. 10, p. 1121, Jul. 2018, doi: 10.3390/rs10071121.

[43] E. Dinnat, D. L. Vine, J. Boutin, T. Meissner, and G. Lagerloef, "Remote sensing of sea surface salinity: Comparison of satellite and *in situ* observations and impact of retrieval parameters," *Remote Sens.*, vol. 11, no. 7, p. 750, Mar. 2019, doi: 10.3390/rs11070750.

[44] D. M. L. Vine and E. Dinnat, "Sensitivity of wide bandwidth radiometer for remote sensing of ocean salinity," *IEEE Trans. Geosci. Remote Sens.*, vol. 60, 2022, Art. no. 5301517, doi: 10.1109/TGRS.2021.3101962.

[45] N. Vinogradova *et al.*, "Satellite salinity observing system: Recent discoveries and the way forward," *Frontiers Mar. Sci.*, vol. 6, p. 243, May 2019, doi: 10.3389/fmars.2019.00243.

[46] R. Lang, Y. D. Zhou, and L. Vine, "Seawater dielectric measurements at 700 MHz," in *Proc. Electromagn. Res. Symp.*, vol. 2, Hangzhou, China, 2022, pp. 25–29.

[47] T. McDougall, P. Barker, and R. Pawlowicz. (Jan. 27, 2015). *Version 3.05*. [Online]. Available: https://help@teos-10.org

David M. Le Vine (Life Fellow, IEEE) received the Ph.D. degree in electrical engineering from the University of Michigan, Ann Arbor, MI, USA.

His background is electrical engineering with specialization in electromagnetic theory and physics. He does his research at the Earth Sciences Division, NASA Goddard Space Flight Center, Greenbelt, MD, USA, where he works to develop techniques for microwave remote sensing of the environment from space. His research has focused on passive remote sensing at the long wavelength end of the microwave spectrum (e.g., L-band) with applications to remote sensing of soil moisture and sea surface salinity (SSS). Examples of this work are the development of the synthetic aperture radiometer, ESTAR, and the launch of AQUARIUS, a National Aeronautics and Space Administration (NASA) Earth System Science Pathfinder (ESSP) mission to measure SSS. He was Deputy Principal Investigator for AQUARIUS. He is a member with the Ocean Salinity Science Team, which continues research on remote sensing of SSS. He is also a member of the Science Team for NASA's Soil Moisture Active Passive (SMAP) mission and the Quality Working Group supporting the European Space Agency (ESA) Soil Moisture and Ocean Salinity (SMOS) mission. His teaching experience includes the Department of Electrical Engineering, University of Maryland, College Park, MD, and an Adjunct Faculty with The George Washington University, Washington, DC, USA.

Dr. Le Vine is a member of the GRSS, Antennas and Propagation Society, the International Union of Radio Science (URSI), and American Geophysical Union. He was a recipient of the IEEE/GRSS Distinguished Achievement Award (2016) and the Golden Florin Award (2014), for contributions to microwave radiometry. He has served on the Geoscience and Remote Sensing Society (GRSS) AdCom and several IEEE committees focused on engineering accreditation.

Roger H. Lang (Life Fellow, IEEE) received the B.S. and M.S. degrees in electrical engineering and the Ph.D. degree in electrophysics from the Polytechnic Institute of Brooklyn, New York, NY, USA, in 1962, 1964, and 1968, respectively.

He did his post-doctoral research in random media under Joe Keller at the Courant Institute of Mathematical Sciences, New York University, New York, NY. He is currently the L. Stanley Crane Professor of engineering and applied science with George Washington University, Washington, DC, USA. He is known for the early development of the discrete scattering model for vegetation. More recently, he has been involved in remote sensing of seawater salinity and soil moisture under vegetation. His research interests include microwave remote sensing, electromagnetic wave propagation, and dielectric measurements.

Dr. Lang received the Distinguished Achievement Award from the IEEE Geoscience and Remote Sensing Society. He is an Active Participant in the IEEE Geoscience and Remote Sensing Society. He was an Associate Editor for Microwave Scattering and Propagation, and the co-chair of the Technical Program Committee for the IGARSS'90 meeting held at College Park, MD, USA, in 1990. He was the Chair of the International URSI Commission F and is a member of the Editorial Board of Waves in Random and Complex Media.

Yiwen Zhou (Member, IEEE) received the B.S. degree in electrical engineering from Southeast University, Nanjing, China, in 2010, and the M.S. and Ph.D. degrees in electrical engineering from The George Washington University (GWU), Washington, DC, USA, in 2012 and 2017, respectively.

He then did his post-doctoral research at GWU, for modeling the radar backscatter from vegetation canopy and the impact of seawater dielectric model on ocean salinity retrieval. He is currently a Research Scientist with Lincoln Agritech Ltd., Lincoln University, Christchurch, New Zealand. His research interests include remote sensing of ocean salinity and soil moisture, scattering model development, accurate dielectric measurements, metamaterials, and microwave medical imaging.

Emmanuel P. Dinnat (Senior Member, IEEE) received an advanced studies degree in instrumental methods in astrophysics and spatial applications and the Ph.D. degree in computer science, telecommunications, and electronics from the University Pierre and Marie Curie, Paris, France, in 1999 and 2003, respectively.

He is currently a Senior Research Scientist with the Center of Excellence in Earth Systems Modeling and Observations (CEESMO), Chapman University, Orange, CA, USA, and the Cryospheric Sciences Laboratory, NASA Goddard Space Flight Center (GSFC), Greenbelt, MD, USA. He is working on the calibration and validation and algorithm improvements for the Soil Moisture and Ocean Salinity (SMOS), Aquarius/SAC-D, and Soil Moisture Active Passive (SMAP) missions. His latest research focuses on high latitude oceanography and the interactions between the cryosphere and oceans. His research interests include active and passive microwave remote sensing, sea surface salinity, scattering from rough surfaces, atmospheric radiative transfer, and numerical simulations.

Thomas Meissner (Senior Member, IEEE) received the B.S. degree in physics from the University of Erlangen-Nürnberg, Erlangen, Germany, in 1983, the M.S. (Diploma) degree in physics from the University of Bonn, Bonn, Germany, in 1987, and the Ph.D. degree in theoretical physics from the University of Bochum, Bochum, Germany, in 1991.

From 1992 to 1998, he conducted his postdoctoral research at the University of Washington, Seattle, WA, USA, the University of South Carolina, Columbia, SC, USA, and Carnegie Mellon University, Pittsburgh, PA, USA, in Theoretical Nuclear and Particle Physics. In 1998, he joined Remote Sensing Systems (RSS), Santa Rosa, CA, USA. Since then, he has been working on the development and refinement of radiative transfer models, calibration, validation, and ocean retrieval algorithms for various microwave instruments [special sensor microwave/imager (SSM/I), Tropical Rainfall Measuring Mission (TRMM) Microwave Imager (TMI), Advanced Microwave Scanning Radiometer for Earth Observing System (AMSR-E), WindSat, Special Sensor Microwave Imager Sounder (SSMIS), Global Precipitation Measurement (GPM) Microwave Imager (GMI), AQUARIUS, Soil Moisture Active Passive (SMAP), Weather System Follow on – Microwave Imager (WSF-MWI), and Copernicus Imaging Microwave Radiometer (CIMR)].

Dr. Meissner has been serving on the review panel for the National Academies' Committee on Radio Frequencies (CORF). As a member of the AQUARIUS Launch, Early Orbit Operations, and Commissioning Team, he was recognized with the NASA Group Achievement Award in 2012. In 2013, he and Frank Wentz received the IEEE Transactions on Geoscience and Remote Sensing Prized Paper Award for the paper describing the RSS ocean radiative transfer model.